

Unconventional spin freezing in the disordered pyrochlore magnet $\text{NaCaCo}_2\text{F}_7$: NMR studies and Monte-Carlo simulations

R. Sarkar,^{1,*} J. W. Krizan,² F. Brückner,¹ E. C. Andrade,^{3,4} S. Rachel,⁵ M. Vojta,⁵ R. J. Cava,² and H.-H. Klauss¹

¹*Institut für Festkörperphysik, Technische Universität Dresden, 01062 Dresden, Germany*

²*Department of Chemistry, Princeton University, Princeton, NJ 08544, USA*

³*Instituto de Física Teórica, Universidade Estadual Paulista,*

Rua Dr. Bento Teobaldo Ferraz, 271 - Bl. II, 01140-070, São Paulo, SP, Brazil

⁴*Instituto de Física de São Carlos, Universidade de São Paulo, C.P. 369, São Carlos, SP, 13560-970, Brazil*

⁵*Institut für Theoretische Physik, Technische Universität Dresden, 01062 Dresden, Germany*

(Dated: April 5, 2016)

We present results of ^{23}Na and ^{19}F nuclear magnetic resonance (NMR) measurements on $\text{NaCaCo}_2\text{F}_7$, a frustrated pyrochlore magnet with a large Curie-Weiss temperature, $\Theta_{\text{CW}} \approx -140$ K, and intrinsic bond disorder. Below 3.6 K both the ^{23}Na and ^{19}F spectra broaden substantially, accompanied by a huge reduction of the NMR signal intensity: These hint at a broad quasi-static field distribution with glassy relaxation dynamics in this regime. The ^{19}F spin-lattice relaxation rate $^{19}(1/T_1)$ exhibits strong low-frequency spin dynamics in a wide temperature range. We attribute the spin freezing to the presence of bond disorder. This is corroborated by large-scale Monte-Carlo simulations of a classical bond-disordered XY model on the pyrochlore lattice. However, the low freezing temperature, together with the very short magnetic correlation length not captured by the simulations, suggest quantum effects to play a decisive role in $\text{NaCaCo}_2\text{F}_7$, possibly placing the material in the proximity of a quantum spin-liquid state.

PACS numbers: 75.10.Nr, 75.40.Gb, 76.60.-k

The pyrochlore lattice is one of the canonical lattices exhibiting geometric frustration. Pyrochlore oxides with the general formula $\text{R}_2\text{T}_2\text{O}_7$ (R = rare earth ion, T = Ti, Sn, Mo, Ir etc.) are characterized by strong frustration of the rare-earth magnetic moments and have been found to display a variety of fascinating low-temperature phases, including classical and quantum spin-ice regimes, quantum order-by-disorder, and exotic spin liquids [1–3].

$\text{NaCaCo}_2\text{F}_7$ is a recently synthesized $\text{A}_2\text{B}_2\text{X}_7$ -type pyrochlore [4]. Here, the B site hosts high-spin Co^{2+} in CoF_6 octahedra, whereas the A site contains a random distribution of Na and Ca ions, giving rise to exchange (bond) disorder for the magnetic degrees of freedom. Bond disorder can lift degeneracies and lead to new unconventional ground states, both long-range ordered [5, 6] and glassy [7–10].

The uniform susceptibility of $\text{NaCaCo}_2\text{F}_7$ displays a Curie-Weiss law with a characteristic temperature $\Theta_{\text{CW}} \approx -140$ K and a moment of $6.1 \mu_{\text{B}}$ per Co, the latter suggesting an orbital contribution in addition to the $S = 3/2$ state of Co^{2+} . Despite the large Θ_{CW} , the material does not display a long-range-ordered magnetic state to temperatures of 0.6 K. Instead, ac and dc susceptibility data indicate a spin freezing at $T_f \approx 2.4$ K [4], yielding a high frustration index of $f = \Theta_{\text{CW}}/T_f \approx 56$. The observed entropy loss at the freezing transition is low, suggesting that magnetic entropy remains present at least down to 0.6 K. Inelastic neutron scattering (INS) results [11] for $\text{NaCaCo}_2\text{F}_7$ show diffuse elastic scattering below 2.4 K. However, its intensity represents only 30% of the total magnetic scattering. The momentum-space structure of the spin correlations below 2.5 meV has

been interpreted in terms of XY-like antiferromagnetic clusters, indicating a local easy-plane anisotropy at low energies, whereas a signal corresponding to collinear correlations was found above this energy. The XY character together with the short detected correlation length of 16 Å [11] appears to be at odds with the theoretical suggestion [6] that bond disorder in an XY pyrochlore magnet induces long-range magnetic order of the so-called ψ_3 type (as opposed to ψ_2 order, which is selected by quantum or thermal fluctuations [12–14]). Hence, the interplay of frustration and quenched disorder in $\text{NaCaCo}_2\text{F}_7$ prompts further studies.

Here we present detailed investigations of $\text{NaCaCo}_2\text{F}_7$ using NMR, thereby microscopically accessing the magnetic order and the low-energy spin dynamics at a μeV energy scale. We characterize the short-range-ordered state at low temperature: It displays substantial NMR line broadening and a wipeout effect characteristic of glassy spin freezing as well as a strong spin-lattice relaxation which is well described by thermally activated low-energy spin fluctuations. We complement these experimental results by large-scale Monte-Carlo simulations of a pyrochlore XY model with bond disorder. The simulation results show that, indeed, bond disorder can lead to a glass-like state without long-range order, qualitatively consistent with experiment. Quantitative comparison between experiment and theory, however, shows physics beyond the classical XY model to be important in $\text{NaCaCo}_2\text{F}_7$. We discuss the intriguing possibility that the material is a bond-disordered quantum spin liquid.

Measurements. Single crystals of $\text{NaCaCo}_2\text{F}_7$ were prepared in an optical floating zone furnace, see Ref. 4 for

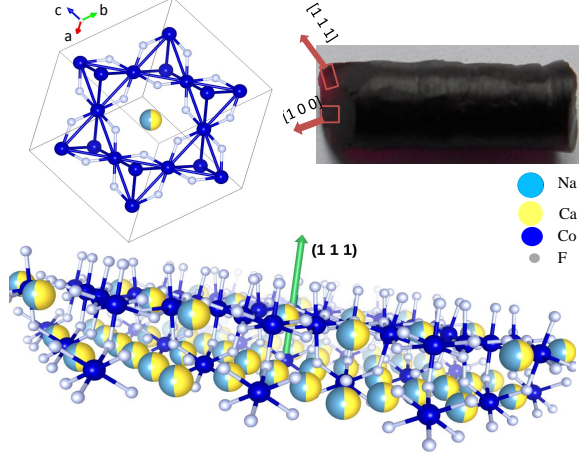


FIG. 1. Top left panel represents the crystallographic view along the $[1\ 1\ 1]$ direction of $\text{NaCaCo}_2\text{F}_7$. Lower panel depicts the side view of the (Na or Ca) layers. The top right part of the figure shows a picture of the single crystal employed.

details. NMR experiments were performed using a Tecmag spectrometer at different frequencies and in a wide temperature range. A crystal of mass 0.89 g was measured, with fields applied along the $[1\ 0\ 0]$, $[1\ 1\ 0]$, and $[1\ 1\ 1]$ directions, see Figure 1. We conducted the ^{23}Na and ^{19}F line shape measurements using a 90° - 90° pulse sequence. For spin-lattice relaxation $1/T_1$ measurements we used the saturation recovery method with a 90° - 90° pulse sequence. $1/T_1$ experiments were performed by exciting the central position of the spectra, for further information see Ref. 15.

^{23}Na NMR spectra. Figure 2 shows ^{23}Na NMR field-sweep spectra at representative temperatures. The spectra can be described by considering two locally nonequivalent Na sites, labelled Na_1 and Na_2 , with different shifts but with similar quadrupolar interaction parameters and nearly equal intensity. The quadrupolar interaction parameters ν_Q are nearly temperature-independent and given by $1.087 \pm 0.013\text{ MHz}$ for both Na sites, Fig. 2b. The appearance of two Na lines indicates that Na nuclei locally experience two different hyperfine fields as is described by the different magnetic shifts, Fig. 2c. At present the microscopic reason for this double-peak structure is not clear; the weak temperature dependence suggests a crystallographic origin related to the distribution of Na and Ca ions on the A site, see Ref. 15. The conclusions drawn below are independent of this feature.

The ^{23}Na spectra broaden gradually upon cooling, and below $\sim 2.9\text{ K}$ distinct structures of the spectrum are smeared out, resulting in a very broad and isotropic line shape. This is the same temperature range where ac susceptibility data show a broad maximum [4]. Such a broad spectrum hints a quasi-static and spatially disordered field distribution in $\text{NaCaCo}_2\text{F}_7$. In contrast, both

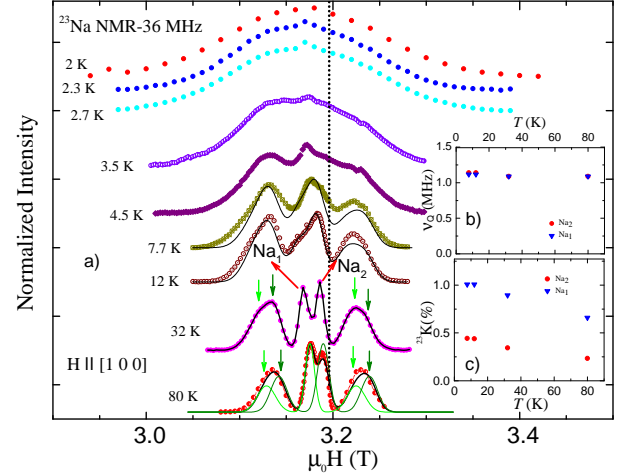


FIG. 2. a) ^{23}Na NMR field-sweep spectra at the frequency of 36 MHz for a field along the $[1\ 0\ 0]$ direction. Lines describe a simulation employing two inequivalent Na sites, with the temperature dependence of the ν_Q and shift values shown in the insets b) and c). Vertical dotted line indicates the position of the Larmor field.

collinear and non-collinear long-range ordered states can be ruled out, because in single crystals those would induce a distinct line splitting in the ordered state [16–18].

^{19}F NMR spectra. In Fig. 3 we show the ^{19}F field-sweep NMR spectra at representative temperatures. Upon lowering the temperature the ^{19}F spectra shift in the low-field side with respect to nonmagnetic ^{19}F reference line with gradual line broadening, and below $\sim 3.6\text{ K}$ the spectra broaden immensely. The effective line width at the FWHM position increases by a factor of 16 when temperature is lowered from 145 K to 2 K. Such a broadening again hints at the presence of a broad distribution of static internal fields.

NMR spin-echo intensities scaled with corresponding temperatures are plotted as a function of temperature in Fig. 4 to have a clear picture of this field distribution. The overall NMR signal intensity, i.e. the area under the curve, is in general inversely proportional to the temperature and proportional to the number of contributing nuclei. The strong loss of signal intensity with lowering the temperature proves that at low temperature not all nuclei contribute to the observed NMR signal. A broad distribution of spin-lattice relaxation rates may lead to such a situation [19–22]. In the present case a robust loss of the ^{19}F and ^{23}Na NMR signal intensities is observed: The signals start to decrease drastically below 20 K, nearly in the same temperature regime where $^{19}(1/T_1)$ starts to increase, see Fig. 5. Hence, the development of slow spin fluctuations and the loss of signal intensity are correlated. The reduction of the NMR signal intensity, the so-called “wipeout effect”, has been widely discussed in the literature in the context of spin-frozen states, and $\text{NaCaCo}_2\text{F}_7$

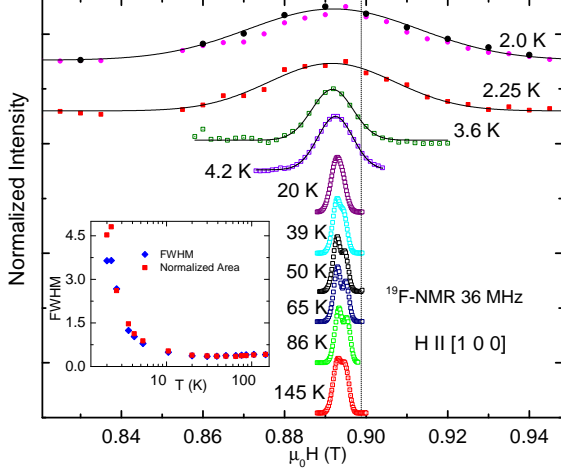


FIG. 3. ^{19}F NMR field-sweep spectra at the frequency of 36 MHz for a field along the $[1\ 0\ 0]$ direction. Lines indicate Gaussian single-peak fit. Inset shows the FWHM and the normalized area as a function of temperature. Vertical dotted line represents the position of the Larmor field (diamagnetic reference).

fits into this picture [19, 21, 23].

The inset of Fig. 4 plots the NMR shift as a function of the bulk susceptibility. This dependence is linear down to 3.6 K, but deviates for lower temperatures. To interpret this we recall that the total shift is the sum of the chemical shift K_0 and the Knight shift K : While K_0 represents the T -independent orbital and conduction-electron contribution, $K = A\chi(T)$ describes the hyperfine coupling to the electronic moments mainly residing on the Co atoms, with A being the hyperfine coupling constant and $\chi(T)$ the magnetic susceptibility. The linear dependence above 3.6 K yields an estimate for the hyperfine coupling of $A = 0.354\text{ KOe}/\mu_B$. The change of slope at 3.6 K reflects an increase of the hyperfine coupling constant and indicates a change of the electronic state from correlated paramagnetic to quasi-static ordered. Such behavior is often observed, e.g., at the formation of correlated electronic states in heavy-fermion systems [24].

Spin relaxation. Next, let us turn our attention to the spin dynamics at very low energies. In Fig. 5 we show the ^{19}F NMR spin-lattice relaxation rate at different fields as a function of temperature. $^{19}(1/T_1)$ values are constant in the temperature range 20–150 K, however below 20 K, $^{19}(1/T_1)$ starts to increase exhibiting a peak at around 2.9 K; we recall that ac and dc susceptibility data also show a broad maximum around this temperature. The spin-spin relaxation rate $^{19}(1/T_2)$ has a similar temperature dependency as $^{19}(1/T_1)$, although $^{19}(1/T_2)$ values are much larger than $^{19}(1/T_1)$. The enhancement of $^{19}(1/T_1)$ below 20 K suggests that $\text{NaCaCo}_2\text{F}_7$ enters into a fluctuating correlated state, i.e., a cooperative paramagnet, before it settles into a frozen state. These

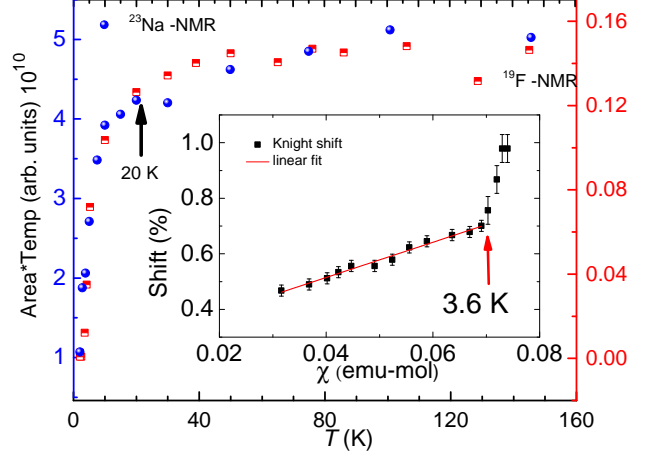


FIG. 4. The wipe-out effect of ^{23}Na and ^{19}F NMR signal. Inset represents the plot of shift vs. susceptibility. The line indicates the linear fit.

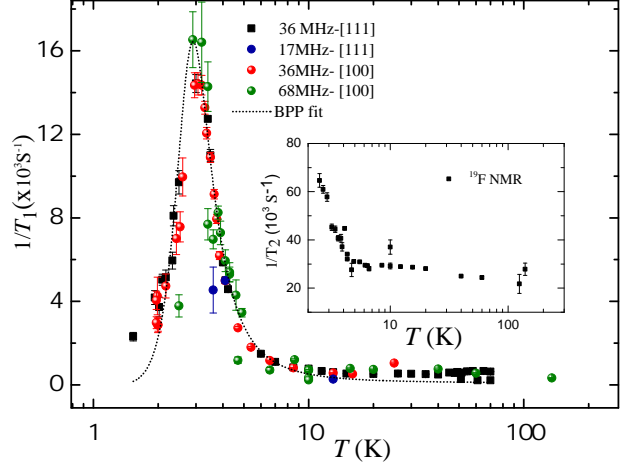


FIG. 5. ^{19}F spin-lattice relaxation rate at different fields and different crystallographic orientations. The dotted line represent a BPP fit as described in the text. Inset shows the temperature dependence of $^{19}(1/T_2)$.

findings are in good agreement with neutron scattering data [11]. We note that the NMR experiments do not show a strong crystallographic orientation dependence of $^{19}(1/T_1)$ in the proximity of the peak, indicating that the spin fluctuations are macroscopically isotropic in nature, consistent with a randomly frozen spin state.

In the past [19, 25, 26] certain classes of spin-frozen systems have been found to display a pronounced low-temperature peak in $1/T_1$ that can be described by the mechanism due to Bloembergen, Purcell, and Pound (BPP) [27]. This assumes a fluctuating hyperfine field $h(t)$ at the nuclear site with autocorrelation function $\langle h(t)h(0) \rangle = h_0^2 \exp(-t/\tau_c)$, where τ_c is the correla-

tion time. In spin-frozen systems, τ_c often exhibits an activated ($\tau_c = \tau_0 \exp(E_a/T)$) or Vogel-Fulcher ($\tau_c = \tau_0 \exp(E_a/(T - T_s))$) behavior [28]. We have chosen $\tau_c = \tau_0 \exp(E_a/T)$ to describe the present data. In the presence of fluctuating hyperfine field, $1/T_1$ as measured by NMR can be represented by the following equation in the framework of the BPP theory:

$$1/T_1(T) = \gamma^2 h_0^2 \tau_c(T) / [1 + \omega_L^2 \tau_c^2(T)], \quad (1)$$

where γ is the nuclear gyromagnetic ratio, and ω_L is the Larmor frequency. This equation yields a peak in $1/T_1$ as function of T once $1/\tau_c$ matches the measured resonance frequency. In Fig. 5 dotted line describes the theoretical description by using this BPP model. Our fit yields $E_a = 1.378 \times 10^{-3}$ eV, $\tau_0 = 8.052 \times 10^{-11}$ s, and $h_0 = 42$ G. These values are in line with ac susceptibility experiments [4] and fit in the framework of spin glasses or spin-glass-like materials [29].

Monte-Carlo simulations. In order to shed light on the glassy freezing, we have performed finite- T Monte-Carlo simulations of a classical pyrochlore XY model with and without bond disorder. In line with earlier work, the clean system orders in the ψ_2 state due to a thermal order-by-disorder effect [12, 13]. Upon introducing strong bond disorder, ψ_2 and ψ_3 configurations are expected to compete [6]. This is analyzed by monitoring the probability distribution of the quantity

$$m_6 = m \cos(6\theta), \quad (2)$$

where the angle $\theta = \tan^{-1}(m_y/m_x)$ describes the in-plane spin direction in a local coordinate frame, such that $m_6 = 1$ (-1) holds for an ideal ψ_2 (ψ_3) state, respectively. Sample results for the m_6 histogram are shown in Fig. 6, with a clear bimodal distribution below the freezing temperature, for details see Ref. 15. We conclude that a long-range ordered ψ_3 state is not realized, at variance with the results of Ref. 6. Instead, bond disorder causes the system to settle into a glassy phase with a spatial mixture of ψ_2 and ψ_3 configurations. This appears qualitatively consistent with the experimental data on $\text{NaCaCo}_2\text{F}_7$.

However, a quantitative comparison shows that our simulations grossly overestimate both the magnetic correlation length and the freezing temperature even for strong bond disorder [15]. Hence, fluctuation effects must be crucial, with two obvious sources, namely quantum effects and fluctuations out of the XY manifold of states due to small crystal field splitting.

Theoretical investigations of “clean” spin models on the pyrochlore lattice have shown that a variety of ordered states compete, and that quantum fluctuations are likely to stabilize quantum spin liquids in parameter regimes near classical phase boundaries [30–32]. Given the large frustration ratio Θ_{CW}/T_f of $\text{NaCaCo}_2\text{F}_7$, we speculate that it may be understood as a quantum spin

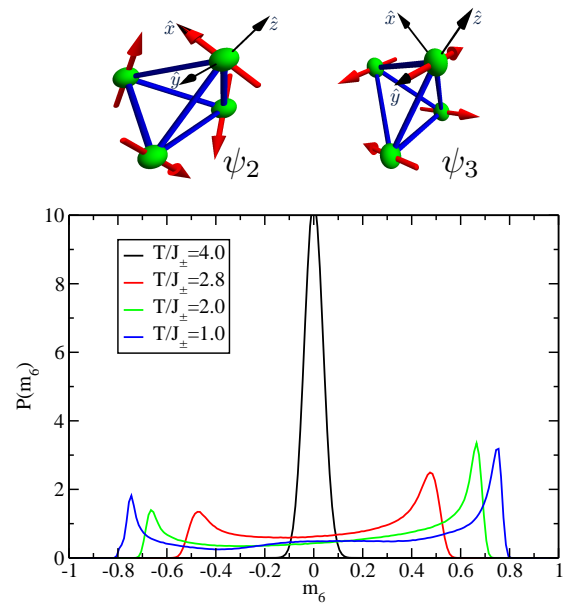


FIG. 6. Top: Schematic representation of the ψ_2 and ψ_3 states of pyrochlore XY magnets. Bottom: Histogram of m_6 (2) – distinguishing ψ_2 and ψ_3 – for the disordered pyrochlore XY model obtained from MC simulations at different temperatures; the freezing temperature is $T_f/J_\pm = 3.15$ (2). The bond strengths are taken from a box distribution with width $W/J_\pm = 2$; for details see text and Ref. 15.

liquid which is driven into a weakly glassy state by bond disorder.

Conclusions. Using NMR measurements we have characterized the magnetism of $\text{NaCaCo}_2\text{F}_7$. It displays (i) a huge reduction of the NMR signal intensity at low temperature, and (ii) a peak in the $^{19}\text{F}(1/T_1)$ vs. T data which can be explained by the thermally activated autocorrelation function. Hence, $\text{NaCaCo}_2\text{F}_7$ represents a frustrated pyrochlore material with unusual static local antiferromagnetic correlations which stabilize a spin-frozen state. Via Monte-Carlo simulations we have qualitatively shown that the glassy freezing can be attributed to quenched structural disorder which in turn induces magnetic bond disorder. The presence of strong low-energy spin fluctuations, as evidenced by neutron scattering [11] and NMR, indicates that quantum effects are crucial for a quantitative understanding of the material.

We acknowledge helpful discussions with K. A. Ross and H. Yasuoka. This research is supported by the Deutsche Forschungsgemeinschaft (DFG) through SFB 1143. The crystal growth work at Princeton University was supported by the US DOE Division of Basic Energy Sciences, grant DE-FG02-08ER46544. E.C.A. was supported by FAPESP (Brazil) Grant No. 2013/00681-8.

* rajibsarkarsinp@gmail.com

- [1] R. Moessner and J. T. Chalker, Phys. Rev. Lett. **80**, 2929 (1998).
- [2] J. S. Gardner, M. J. P. Gingras, and J. E. Greedan, Rev. Mod. Phys. **82**, 53 (2010).
- [3] C. Lacroix, P. Mendels, and F. Mila, Introduction to Frustrated Magnetism: Materials, Experiments, Theory, **Vol. 164** (Springer, Berlin, Heidelberg, 2011).
- [4] J. W. Krizan and R. J. Cava, Phys. Rev. B **89**, 214401 (2014).
- [5] V. S. Maryasin and M. E. Zhitomirsky, Phys. Rev. Lett. **111**, 247201 (2013).
- [6] V. S. Maryasin and M. E. Zhitomirsky, Phys. Rev. B **90**, 094412 (2014).
- [7] T. E. Saunders and J. T. Chalker, Phys. Rev. Lett. **98**, 157201 (2007).
- [8] A. Andreanov, J. T. Chalker, T. E. Saunders, and D. Sherrington, Phys. Rev. B **81**, 014406 (2010).
- [9] H. Shinaoka, Y. Tomita, and Y. Motome, Phys. Rev. Lett. **107**, 047204 (2011).
- [10] H. J. Silverstein, K. Fritsch, F. Flicker, A. M. Hallas, J. S. Gardner, Y. Qiu, G. Ehlers, A. T. Savici, Z. Yamani, K. A. Ross, B. D. Gaulin, M. J. P. Gingras, J. A. M. Paddison, K. Foyevtsova, R. Valenti, F. Hawthorne, C. R. Wiebe, and H. D. Zhou, Phys. Rev. B **89**, 054433 (2014).
- [11] K. A. Ross, J. W. Krizan, J. A. Rodriguez-Rivera, R. J. Cava, and C. L. Broholm, Phys. Rev. B **93**, 014433 (2016).
- [12] M. E. Zhitomirsky, M. V. Gvozdkova, P. C. W. Holdsworth, and R. Moessner, Phys. Rev. Lett. **109**, 077204 (2012).
- [13] L. Savary, K. A. Ross, B. D. Gaulin, J. P. C. Ruff, and L. Balents, Phys. Rev. Lett. **109**, 167201 (2012).
- [14] M. E. Zhitomirsky, P. C. W. Holdsworth, and R. Moessner, Phys. Rev. B **89**, 140403 (2014).
- [15] See Supplemental Material at [URL will be inserted by publisher] for a description of spectra analysis and theory.
- [16] R. Melzi, S. Aldrovandi, F. Tedoldi, P. Carretta, P. Millet, and F. Mila, Phys. Rev. B **64**, 024409 (2001).
- [17] Y. Tokunaga, Y. Saito, H. Sakai, S. Kambe, N. Sanada, R. Watanuki, K. Suzuki, Y. Kawasaki, and Y. Kishimoto, Phys. Rev. B **84**, 214403 (2011).
- [18] K. Kitagawa, N. Katayama, K. Ohgushi, M. Yoshida, and M. Takigawa, J. Phys. Soc. Jpn. **77**, 114709 (2008).
- [19] N. J. Curro, P. C. Hammel, B. J. Suh, M. Hückler, B. Büchner, U. Ammerahl, and A. Revcolevschi, Phys. Rev. Lett. **85**, 642 (2000).
- [20] A. W. Hunt, P. M. Singer, A. F. Cederström, and T. Imai, Phys. Rev. B **64**, 134525 (2001).
- [21] A. W. Hunt, P. M. Singer, K. R. Thurber, and T. Imai, Phys. Rev. Lett. **82**, 4300 (1999).
- [22] P. Mendels, A. Keren, L. Limot, M. Mekata, G. Collin, and M. Horvatić, Phys. Rev. Lett. **85**, 3496 (2000).
- [23] D. E. MacLaughlin and H. Alloul, Phys. Rev. Lett. **36**, 1158 (1976).
- [24] M. Jiang, N. J. Curro, and R. T. Scalettar, Phys. Rev. B **90**, 241109 (2014).
- [25] N. J. Curro, A. P. Dioguardi, N. ApRoberts-Warren, A. C. Shockley, and P. Klavins, New Journal of Physics **11**, 075004 (2009).
- [26] B. J. Suh, P. C. Hammel, M. Hückler, B. Büchner, U. Ammerahl, and A. Revcolevschi, Phys. Rev. B **61**, R9265 (2000).
- [27] N. Bloembergen, E. M. Purcell, and R. V. Pound, Phys. Rev. **73**, 679 (1948).
- [28] J. Schmalian and P. G. Wolynes, Phys. Rev. Lett. **85**, 836 (2000).
- [29] Y. Yeshurun, J. L. Tholence, J. K. Kjems, and B. Wanklyn, Journal of Physics C: Solid State Physics **18**, L483 (1985).
- [30] L. Savary and L. Balents, Phys. Rev. Lett. **108**, 037202 (2012).
- [31] H. Yan, O. Benton, L. Jaubert, and N. Shannon, arXiv:1311.3501.
- [32] M. J. P. Gingras and P. A. McClarty, Rep. Prog. Phys. **77**, 056501 (2014).